



## On the Reliability of Half-Cell Tests for Monovalent ( $\text{Li}^+$ , $\text{Na}^+$ ) and Divalent ( $\text{Mg}^{2+}$ , $\text{Ca}^{2+}$ ) Cation Based Batteries

D. S. Tchitchekova,<sup>a,b</sup> D. Monti,<sup>b,c</sup> P. Johansson,<sup>b,c</sup> F. Bardé,<sup>d</sup> A. Randon-Vitanova,<sup>e</sup> M. R. Palacín,<sup>a,b,\*</sup> and A. Ponrouch<sup>a,b,\*</sup>

<sup>a</sup>Institut de Ciència de Materials de Barcelona, ICMAB-CSIC, Campus de la UAB 08193 Bellaterra, Catalonia, Spain

<sup>b</sup>ALISTORE ERI European Research Institute

<sup>c</sup>Department of Physics, Chalmers University of Technology, SE-412 96 Göteborg, Sweden

<sup>d</sup>Toyota Motor Europe, Research and Development 3, Advanced Technology 1, Technical Centre, B-1930 Zaventem, Belgium

<sup>e</sup>Honda R&D Europe, 63073 Offenbach, Germany

A comprehensive study is reported entailing a comparison of Li, Na, K, Mg, and Ca based electrolytes and an investigation of the reliability of electrochemical tests using half-cells. Ionic conductivity, viscosity, and Raman spectroscopy results point to the cation-solvent interaction to follow the polarizing power of the cations, i.e.  $\text{Mg}^{2+} > \text{Ca}^{2+} > \text{Li}^+ > \text{Na}^+ > \text{K}^+$  and to divalent cation based electrolytes having stronger tendency to form ion pairs – lowering the cation accessibility and mobility. Both increased temperature and the use of anions with delocalized negative charge, such as TFSI, are effective in mitigating this issue. Another factor impeding the divalent cations mobility is the larger solvation shells, as compared to those of monovalent cations, that in conjunction with stronger solvent - cation interactions contribute to slower charge transfer and ultimately a large impedance of Mg and Ca electrodes. An important consequence is the non-reliability of the pseudo-reference electrodes as these present both significant potential shifts as well as unstable behaviors. Finally, experimental protocols in order to achieve consistent results when using half-cell set-ups are proposed.

© The Author(s) 2017. Published by ECS. This is an open access article distributed under the terms of the Creative Commons Attribution 4.0 License (CC BY, <http://creativecommons.org/licenses/by/4.0/>), which permits unrestricted reuse of the work in any medium, provided the original work is properly cited. [DOI: 10.1149/2.0411707jes] All rights reserved.



Manuscript submitted January 25, 2017; revised manuscript received March 20, 2017. Published May 2, 2017.

Although the lithium-ion battery is currently being considered as the most promising technology for electric vehicle propulsion, the development of alternative and complementary battery chemistries and technologies is of great importance, especially aiming at large-scale applications, i.e. the grid for which the cost in \$/kWh and sustainability are crucial indicators. Indeed, the implementation of lithium based technology at large scale faces a significant challenge, since the controversial debates on lithium availability and cost cannot be overlooked. Amongst several chemistries possible the most appealing alternatives involve the use of sodium (Na), magnesium (Mg) or calcium (Ca) for mainly two reasons. The prime is the abundance of the raw materials, i.e. Na, Mg, and Ca being the 6<sup>th</sup>, 8<sup>th</sup>, and 5<sup>th</sup> most abundant elements in the Earth's crust, vs. 25<sup>th</sup> for Li, making them 20 to 50 times cheaper than Li, e.g. \$5000/ton, \$135–165/ton, \$265/ton, and \$100/ton for  $\text{Li}_2\text{CO}_3$ ,  $\text{Na}_2\text{CO}_3$ ,  $\text{MgO}_2$ , and  $\text{CaCO}_3$ ,<sup>1</sup> respectively. Performance wise, the low cost alternatives of Na, Mg, and Ca technologies would also benefit from high standard reduction potentials, ca.  $-2.71$ ,  $-2.37$ , and  $-2.87$  V vs. SHE for Na, Mg, and Ca, respectively, as compared to  $-3.04$  V for Li, and large theoretical electrochemical capacities, both gravimetric and volumetric, for the metal electrodes (Fig. 1).

Sodium metal anodes are already used in the liquid state (m.p.  $\sim 97^\circ\text{C}$ ) in the Na/S technology<sup>2</sup> and room-temperature Na-ion technology is currently intensively investigated with hundreds of papers appearing per year, with progress being summarized in several review papers amongst which<sup>3–5</sup> are the most recent. For Mg and Ca metal anodes, the situation is radically different. For the Mg battery technology, proof-of-concept was achieved as late as in 2000,<sup>6</sup> although its practical development has been hampered by some fundamental challenges that are gradually being overcome.<sup>7–9</sup> For Ca, the viability of metal electrodeposition has only recently been achieved<sup>10</sup> and a few studies on possible cathode materials have started to appear in 2015–2016<sup>11–19</sup> being to the best of our knowledge the exhaustive list. Since the Mg and Ca cations are divalent, the amount of ions that must react in order to achieve a certain electrochemical capacity is half compared to the monovalent  $\text{Li}^+$  and  $\text{Na}^+$ .

For all battery chemistries, a reliable electrochemical set-up is essential to evaluate basic properties, especially at the development stage of new electrodes and electrolytes, such as capacity and safe operation potential. Half-cell configurations with typically only two electrodes, i.e. with metal electrode as both the counter (CE) and the reference (RE) electrode, were commonly adopted for Li, Na, Mg cells, and more recently also for Ca based cells. However, several requirements need to be fulfilled in order to achieve reliable results for half-cell set-ups (Fig. 2). The main conditions for the CE are: i) high surface area and/or high reaction kinetics in order to allow for complete reaction at the working electrode (WE) and ii) the reaction occurring at the CE should not affect/contaminate the system. For the RE the following properties should hold: i) non-polarizable, i.e. a small residual current ( $< 50$  pA) flowing should not affect the potential, ii) reliable and stable potential with time (ideally, reproducible to about one millivolt), and iii) low impedance ( $< a$  few  $\text{k}\Omega$ ). Although these conditions are, at least satisfactorily, met in Li half-cells,<sup>20</sup> recent studies point to several issues associated with the use of Na metal CEs and REs.<sup>21–24</sup> No extensive studies have been made in order to evaluate the reliability of Mg and Ca half-cell configurations. Undeniably, the poor

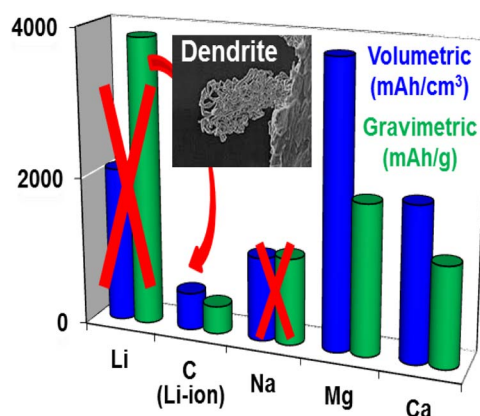


**Figure 1.** Theoretical gravimetric and volumetric capacities for different anodes: metals and Li-ion.

\*Electrochemical Society Member.

<sup>†</sup>E-mail: [aponrouch@icmab.es](mailto:aponrouch@icmab.es)

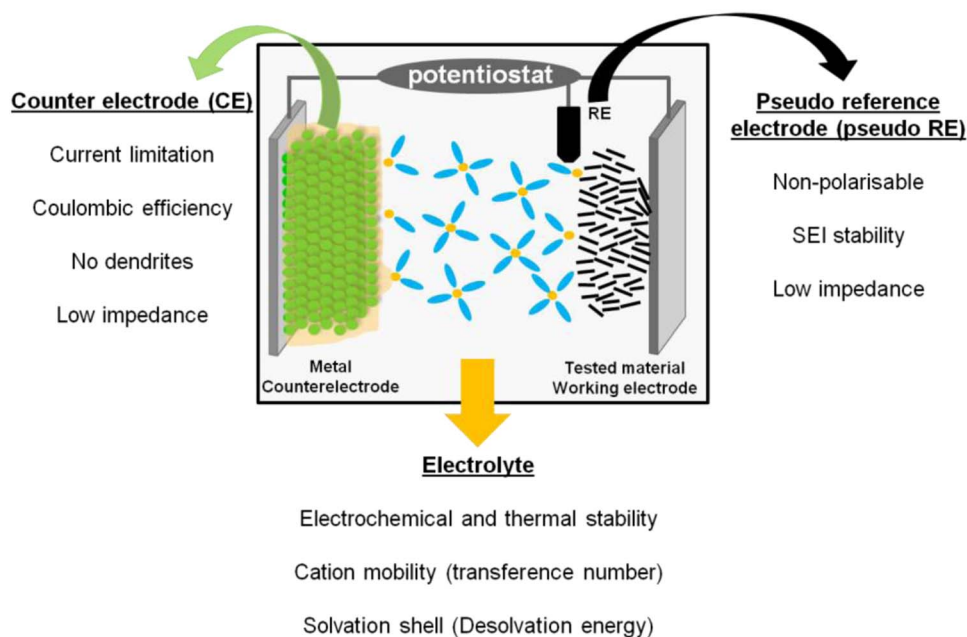


**Figure 2.** Scheme of a half-cell configuration with the main properties required for reliable CEs and REs.

divalent cation mobility within the electrolyte is an important limiting factor in Ca based cells, as reported in Ref. 10, but to the best of our knowledge, there is currently no systematic investigation comparing the transport properties of monovalent and divalent cations in electrolytes. In the present work, we have studied the physicochemical properties of electrolytes based on monovalent ( $\text{Li}^+$  and  $\text{Na}^+$ ) and divalent ( $\text{Ca}^{2+}$  and  $\text{Mg}^{2+}$ ) cation salts. The main parameters affecting the half-cell electrochemical tests for Na, Mg and Ca are discussed and compared against results for the corresponding Li systems.

### Experimental

All electrolytes used consisted of either 0.1 M or 1 M of Li, Na, Mg, and Ca salts, with anions of  $\text{ClO}_4^-$  or TFSI,  $[(\text{CF}_3\text{SO}_2)\text{N}]^-$ , in a 50:50 wt% mixture of propylene carbonate (PC, Aldrich, anhydrous 99.7%) and ethylene carbonate (EC, Aldrich, anhydrous 99.0%). The solvents were stored in an argon filled glove box and were used as received. The salts were vacuum dried at moderate temperatures prior to usage. The water content in the electrolytes was measured by Karl-Fisher titration and found to be lower than 30 ppm in all cases.

These electrolytes were chosen as EC and PC benefit from large thermal stability windows, between ca.  $-90$  and  $240^\circ\text{C}$ ,<sup>25</sup> which makes them suitable for tests in a wide range of temperatures. Besides, the high dielectric constants and donor numbers of EC and PC favor salts dissociation and thus create excellent model electrolytes for comparing the influence of different cations.

The ionic conductivities of the electrolytes were measured with an MCM 10 Multiplexed Conductivity Meter (BioLogic) over a wide range of temperatures. The viscosities of the electrolytes were measured with a RheoStress RS600 Rheometer (HAAKE) at 25, 50, and  $75^\circ\text{C}$ .

Raman spectroscopy was performed on 1 mL of each electrolyte sample placed in a cylindrical cuvette, sealed with paraffin tape inside an argon filled glove-box, at 20, 40, and  $80^\circ\text{C}$  as controlled by a Peltier element. All measurements were made using a Bruker MultiRAM FT-Raman spectrometer with a nitrogen-cooled germanium detector and a resolution of  $2\text{ cm}^{-1}$ . In order to optimize the signal-to-noise ratio and avoid luminescence, a Nd-YAG (1064 nm) laser was used as excitation source at an operating power of 500 mW and the spectra were averaged over 1000 scans. For a few selected electrolytes band-fitting and deconvolution were made in order to analyze in detail the cation coordination.

Each band used for analysis was fitted using Voigt functions and two models were elaborated upon by considering the position, the width, and the mix of Gaussian and Lorentzian band-shape contributions (successively fixed). EC, NaEC, LiEC, KEC, MgEC and CaEC structures were constructed and optimized at the B3LYP/6-311+G\* level of theory. All structures were verified to be minima from their Hessians. The frequencies and Raman activities were then calculated. All calculations were made using Gaussian 09.<sup>26</sup>

Electrochemical impedance spectroscopy (EIS) and cyclic voltammetry (CV) were performed in two- and three-electrode Swagelok cells, respectively. Lithium (foil from Chemetal), sodium (Aldrich, 99.95%), magnesium (Aldrich, >99.5%), and calcium (Alfa Aesar, 99.5%) metal electrodes were used as CE and RE. Impedance measurements were done under potentiostatic control (PEIS) by applying perturbation amplitudes of 10 mV with frequencies ranging from 20 kHz to 10 mHz. PEIS measurements were performed after 2 h open circuit potential (OCP). The use of symmetric cells with well aligned electrodes constitutes the most reliable experimental setup<sup>27</sup> allowing to minimize possible impedance distortion associated with geometrical misalignment or electrical asymmetry. All electrochemical tests were performed using a Bio-Logic MPG2 potentiostat and twin cells were assembled in order to ensure reproducibility of results.

### Results and Discussion

**Physico-chemical properties of electrolytes.—Conductivity and viscosity.**—The ionic conductivities of the 0.1 M electrolytes containing  $\text{LiClO}_4$ ,  $\text{NaClO}_4$ ,  $\text{Mg}(\text{ClO}_4)_2$ , or  $\text{Ca}(\text{ClO}_4)_2$  in  $\text{EC}_{0.5}:\text{PC}_{0.5}$ , between  $-10$  and  $120^\circ\text{C}$ , are directly proportional to the amount of free charge carriers in the solution (Fig. 3). The 0.1 M Mg and Ca based electrolytes exhibit about twice higher ionic conductivities, e.g. 3.6 and 3.4 mS/cm at  $25^\circ\text{C}$ , respectively, than the Li and Na based, e.g. 1.7 and 1.5 mS/cm at  $25^\circ\text{C}$ , respectively. At these, for battery purposes, rather low concentrations almost total salt dissociation is expected, and the difference in conductivities between monovalent and divalent cation based electrolytes might simply be explained by the differences in the moles of charge carriers created combined with the total unit charges.

For the 1 M electrolytes a completely different trend can be observed; indeed the Li and Na based electrolytes yield the higher conductivities at 6.3 and 6.9 mS/cm at  $25^\circ\text{C}$ , respectively, while for

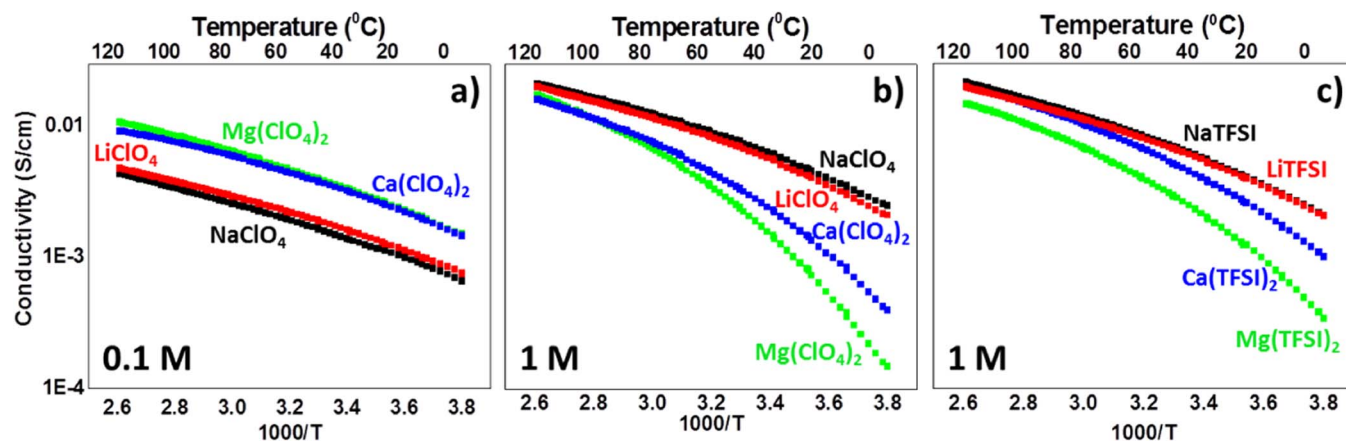


**Figure 3.** Arrhenius plot of the electrolyte ionic conductivities.

Mg and Ca ca. 1.9 and 2.8 mS/cm at 25°C are achieved (Fig. 3b). Given the tenfold increase in salt concentration from 0.1 to 1 M, the ionic conductivities do not increase in a similar fashion indicating a lower amount of free charge carriers and/or decreased ion mobility. This effect is stronger for the divalent cation based electrolytes, where the ion conductivity even decreases from 0.1 M to 1 M. As expected, due to the higher polarizing power of  $\text{Mg}^{2+}$  when compared with  $\text{Ca}^{2+}$ , the tendency is more obvious for the Mg based electrolytes and in agreement with the overall lower conductivities of the Mg based electrolytes as compared to the Ca analogues (Fig. 3b), a difference enhanced at low temperatures, but almost disappearing at 100°C. Indeed, at  $-10^\circ\text{C}$  the 1 M electrolyte ionic conductivities are ca. 1.2 and 2.1 mS/cm, respectively, while at 100°C both have conductivities of ca. 12.6 mS/cm.

In order to study the influence, if any, of the anion, similar experiments were carried out using LiTFSI, NaTFSI, Mg(TFSI)<sub>2</sub> and Ca(TFSI)<sub>2</sub> salt based electrolytes. For 0.1 M the conductivities are comparable, though slightly lower (not shown), and the same is true for 1 M Li and Na (Fig. 3c). However, the 1 M studies show the Mg(TFSI)<sub>2</sub> and Ca(TFSI)<sub>2</sub> based electrolytes to apparently be slightly less affected by ion pair formation and/or low ion mobility. These differences are only observable at low temperatures with 1.9 and 3.4 mS/cm at  $-10^\circ\text{C}$ , respectively for Mg(TFSI)<sub>2</sub> and Ca(TFSI)<sub>2</sub>, and only 1.2 and 2.1 mS/cm for Mg(ClO<sub>4</sub>)<sub>2</sub> and Ca(ClO<sub>4</sub>)<sub>2</sub>. This is in agreement with a more delocalized negative charge for TFSI and therefore being less prone to ion pair formation.<sup>28</sup>

Different trends are observed for the viscosity of monovalent and divalent cation based electrolytes. For the Li and Na based electrolytes, viscosities of 1–3 cP are obtained for the 0.1 M and 1 M at 25, 50, and 75°C (Fig. 4), but for the Mg and Ca based electrolytes it fluctuates with both concentration and temperature. As an example at 25°C the 0.1 M Mg(ClO<sub>4</sub>)<sub>2</sub> and Ca(ClO<sub>4</sub>)<sub>2</sub> based electrolytes have viscosities of about 3 cP, while at the same temperature the 1 M electrolytes exhibit about 95 and 70 cP, respectively. This confirms a significantly lower ion mobility, which is inversely proportional to the viscosity, to contribute to the lower ionic conductivities, possibly together with a substantial degree of ion pair formation. With increasing temperature the viscosities decrease to 20–25 cP at 50°C and below 10 cP at 75°C for 1 M Mg and Ca based electrolytes.

**Raman spectroscopy.**—Raman spectroscopy was performed in order to obtain insight into the solvation shell composition for the monovalent and divalent cations and any possible influence on the cation mobility. The spectra obtained for the TFSI based electrolytes all exhibit a band assignable to cation - EC species (“Cat-EC”) at about 900–910  $\text{cm}^{-1}$ , shifted ca. 4–15  $\text{cm}^{-1}$  from the main band at ca. 894  $\text{cm}^{-1}$  assigned to the EC breathing mode (Figs. 5b, 5d, and 5f). The shift increases in the order of increasing charge/radius ratio:  $\text{K}^+ < \text{Na}^+ < \text{Li}^+ < \text{Ca}^{2+} < \text{Mg}^{2+}$ , indicative of a progressively stronger

cation-solvent interaction, observed for both EC and EC<sub>0.5</sub>:PC<sub>0.5</sub> based electrolytes.

For the 1 M EC and EC<sub>0.5</sub>:PC<sub>0.5</sub> electrolytes a strong broad feature associated to the TFSI anion all breathing mode, an excellent probe for ion-ion interactions, is present at 730–760  $\text{cm}^{-1}$  (Figs. 5c and 5e),<sup>29,30</sup> and deconvolution results in bands at 742  $\text{cm}^{-1}$  (“free” TFSI) and at 744–747  $\text{cm}^{-1}$  corresponding to ion-ion interaction (“Cat-TFSI”) with the position dependent on the cation and most noticeable for the 1 M Ca(TFSI)<sub>2</sub> electrolyte, but also discernible for the 1 M Mg(TFSI)<sub>2</sub> electrolyte. This suggests that in 1 M divalent cation based electrolytes ion pairs form, reducing the number of effective charge carriers consistent with the significantly lower ionic conductivities observed.

Overall the cations are preferentially solvated by EC and the analysis of the Raman spectra allow us to deduce the solvation numbers (SNs) using calculated Raman activities (Table I) - with the exception of 0.1 M KTFSI due to proximity of the two bands and hence the deconvolution uncertainty (Table II). In general, the 0.1 M electrolytes present higher SNs than the 1 M electrolytes. Also, the SNs for the divalent cations (Ca and Mg) based electrolytes are larger than for the monovalent cation (Li, Na, and K) based electrolytes. The higher SNs for 0.1 M can be explained by the larger anion/cation ratio or anion availability allowing the formation of larger complexes. The

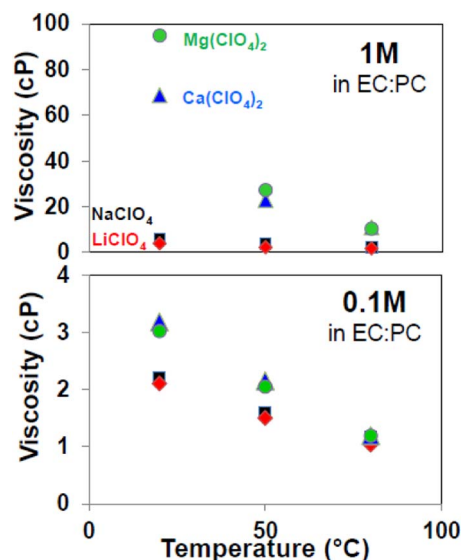


**Figure 4.** Viscosities of the 0.1 and 1 M  $\text{MClO}_4^-$  based electrolytes at 25, 50 and 75°C.

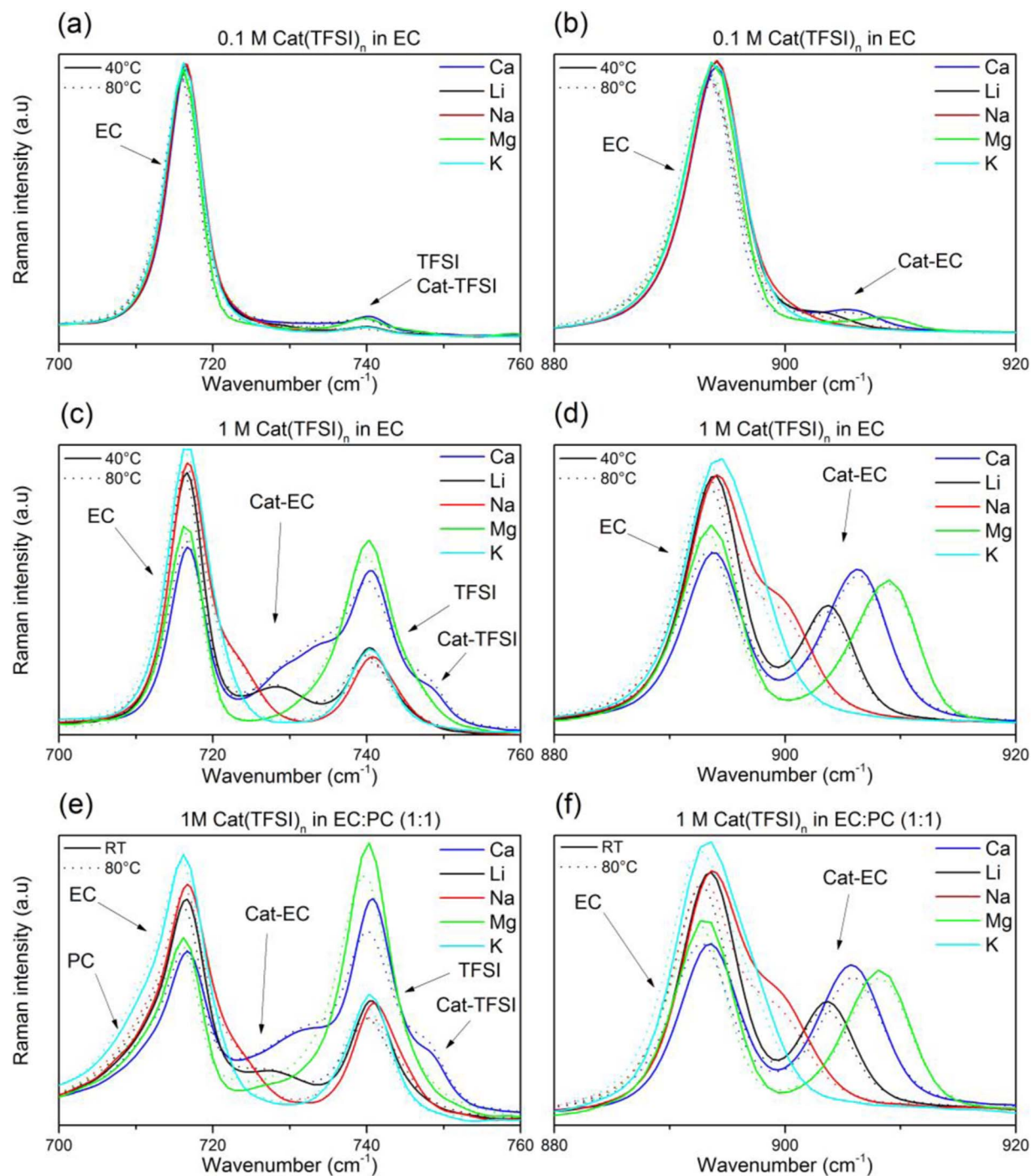


**Figure 5.** Raman spectra of the LiTFSI, NaTFSI, KTFSI, Ca(TFSI)<sub>2</sub>, and Mg(TFSI)<sub>2</sub> based electrolytes: (a) and (b) 0.1 M in EC; (c) and (d) 1 M in EC; (e) and (f) 1 M in EC<sub>0.5</sub>:PC<sub>0.5</sub>., at RT, 40, and 80°C in order to study the cation solvation shell variations.

**Table I.** Fitted location of pure EC and solvated EC bands with K, Na, Li, Ca, and Mg, including Raman activities (R.A.).

	$\nu_{\text{EC}}$	$\nu_{\text{K-EC}}$	$\nu_{\text{Na-EC}}$	$\nu_{\text{Li-EC}}$	$\nu_{\text{Ca-EC}}$	$\nu_{\text{Mg-EC}}$
Raman activities (R.A.) [amu Å <sup>-4</sup> ]	13.7	19.4	18.3	18.3	18.5	19.3
Fitted band location [cm <sup>-1</sup> ]	894	897	900	904	906	908

**Table II.** Solvation numbers, determined by Raman spectroscopy at RT, for 0.1 M and 1 M of KTFSI, LiTFSI, NaTFSI, Mg(TFSI)<sub>2</sub> and Ca(TFSI)<sub>2</sub> in EC and EC<sub>0.5</sub>:PC<sub>0.5</sub> electrolytes.

Cation	0.1 M salt in EC	1 M salt in EC	1 M salt in EC:PC
K <sup>+</sup>	/	2.2	1.2
Na <sup>+</sup>	5.2	3.2	2.9
Li <sup>+</sup>	5.5	2.9	2.1
Ca <sup>2+</sup>	6.7	5.3	3.3
Mg <sup>2+</sup>	6.1	4.6	2.7

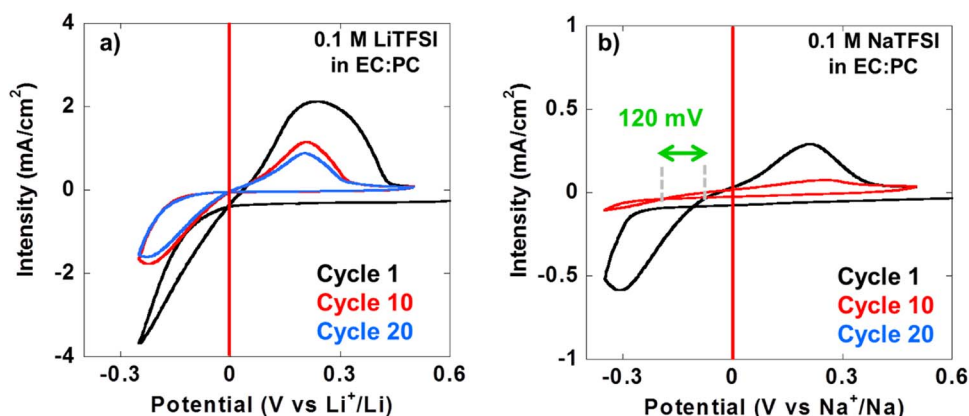


**Figure 6.** CVs (20 mV/s, 25°C) obtained in three-electrode Swagelok cells using (a) 0.1 M LiTFSI or (b) 0.1 M NaTFSI in EC<sub>0.5</sub>:PC<sub>0.5</sub>.

lower SNs for EC in EC<sub>0.5</sub>:PC<sub>0.5</sub> as compared to EC (Table II) is most probably due to PC contributing to the solvation shell as well.

Modifying the temperature to 80°C slightly shifts every free EC and free TFSI bands to lower wavenumber for about 2 cm<sup>-1</sup>. It means that the modification of the surrounding induced by the augmentation of temperature affects these modes and therefore less energy is required for these bonds to vibrate. However, the temperature modification on solvated EC with any cation does not impact the band location meaning that 80°C is not high enough to modify significantly the solvation shell or the distance or/and bond strength between EC and the cation.

The differences in the solvation shells and in the tendency of ion pair formation are both in good agreement with the much higher viscosities and lower ionic conductivities for the 1 M Mg and Ca based electrolytes and confirm the lower cation mobilities in the divalent metal systems (Mg and Ca) as compared to the monovalent (Li and Na), ultimately resulting in lower cation transference numbers affecting the electrochemical behavior. Li<sup>+</sup> transference numbers of 0.2–0.4 are common<sup>31</sup> and for Mg<sup>2+</sup> they can be <0.1,<sup>32</sup> and hence, with the solvated cations less mobile than the anions, the mass transport within the electrolyte can be considered a most crucial parameter for the development of any divalent cation based battery technology.

**Electrochemical behavior of metal electrodes.—Reliability of Li, Na and Ca counter electrodes.—**The electrochemical behavior of Li and Na metal anodes with respect to reversibility and coulombic efficiency of metal plating and stripping were studied by means of CV using stainless steel plungers as WEs and the 0.1 M TFSI based electrolytes (Fig. 6). The coulombic efficiency of the plating/stripping process, defined as the ratio between the charge passed during plating (reduction) and stripping (oxidation), shows for the first cycle to be higher for Li (ca. 60%) than for Na (ca. 40%). For the subsequent cycles, the electrochemical behavior of the metal anodes differs substantially; for Li both the plating over-potential and coulombic efficiency of plating/stripping stabilizes at ca. 80 mV and 75%, respectively, while the Na plating over-potential slowly increases upon cycling and in addition a continuous shift toward negative potentials of the whole voltammogram is observed. Indeed, even during the first cycle the Na plating/stripping is not centered at 0 V vs. Na<sup>+</sup>/Na, but rather at ca. -50 mV vs. Na<sup>+</sup>/Na. This initial potential shift increases upon cycling and, eventually, no more Na plating can be observed for the same lower cutoff potential – clearly pointing toward important instabilities of the Na RE. This will be discussed in more detail in the next section.

As expected, the coulombic efficiencies are dependent on the electrolyte salt concentration – decreasing with increased salt concentration, likely due to the enhanced current density which favors inhomogeneous metal growth (not shown). However, since CV is hardly representative for battery cycling, symmetric Li//Li and Na//Na cells were assembled and tested using galvanostatic cycling with potential

limitation (GCPL) at 0.05 mA/cm<sup>2</sup> (Fig. 7). The end of life of the Na//Na symmetric cell is reached after less than 50 h cycling. The extremely low coulombic efficiency of the Na plating stripping is a major drawback, and thus results obtained from long term cycling tests using Na half-cells should be considered with care as extrapolation to behavior in full cell can be significantly misleading.

Unfortunately, Ca plating does not occur under the conditions tested so far using TFSI or ClO<sub>4</sub><sup>-</sup> based electrolytes and Mg plating was not successful either. However, Ca plating has been reported to be feasible in BF<sub>4</sub><sup>-</sup> based electrolytes.<sup>10</sup> Using an electrolyte of 0.45 M Ca(BF<sub>4</sub>)<sub>2</sub> in EC<sub>0.5</sub>:PC<sub>0.5</sub> in order to be able to compare the efficiency of the plating/stripping process to Li and Na, it appears to be fairly reversible with a low voltage hysteresis between plating and stripping and good coulombic efficiency after the first cycle (ranging from ca. 40% to more than 85% depending on the lower cut off voltage) (Fig. 8a). However, a significant potential shift is observed; the plating/stripping process is centered at ca. -1 V vs. Ca metal pseudo RE. In order to better understand this potential shift, a Li metal pseudo RE was employed resulting in a plating and stripping centered near 0 V vs. Li pseudo RE (Fig. 8b). However, the coulombic efficiency is significantly lowered and the presence of two stripping peaks at ca. 0.16 and 0.27 mV vs. Li pseudo RE is indicative of Li<sup>+</sup> contamination of the electrolyte from the RE, further confirmed by an increasing cathodic current upon cycling. Nonetheless, during the first cycle Ca is plated and stripped at a potential very close to its standard potential, i.e. -2.87 V vs. SHE or 0.17 V vs. Li<sup>+</sup>/Li, allowing us to conclude that the potential shift is not related to any electrolyte based ohmic drop or poor reference electrode positioning associated with the use of Swagelok cell, but is rather an intrinsic property of the Ca pseudo RE. A significant ohmic drop would affect both the anodic and cathodic currents in opposite direction, resulting in a separation

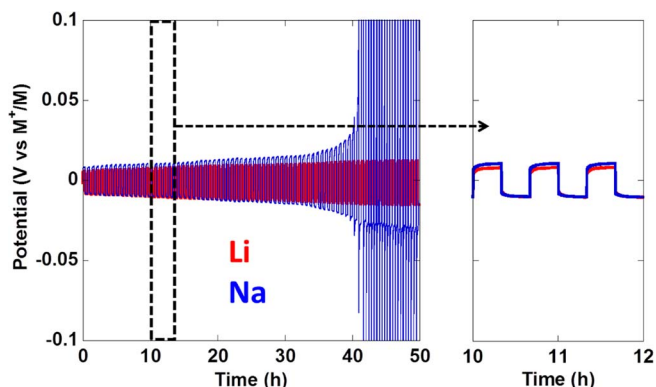


**Figure 7.** Charge/discharge curves (0.05 mA/cm<sup>2</sup>) of symmetric Li//Li and Na//Na cells cycled at 25°C using 0.1 M LiTFSI or NaTFSI in EC<sub>0.5</sub>:PC<sub>0.5</sub>.

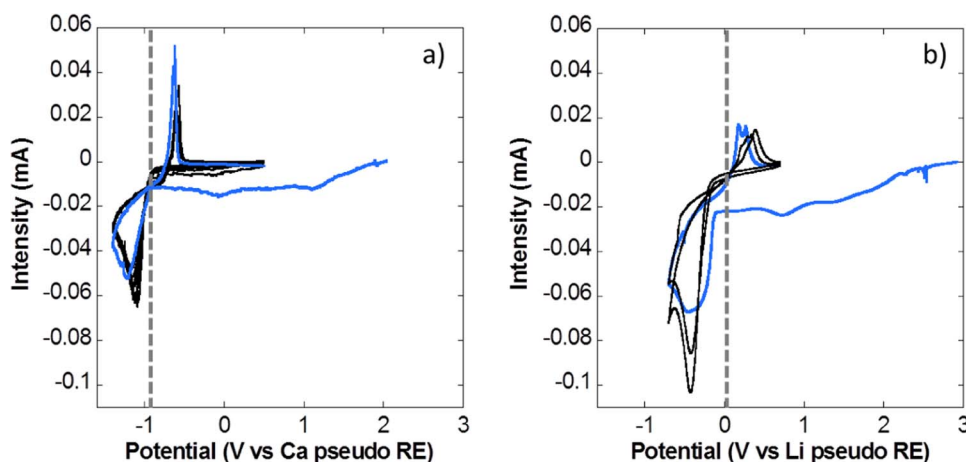


**Figure 8.** CVs (0.1 mV/s) obtained in three-electrode Swagelok cells with 0.45 M  $\text{Ca}(\text{BF}_4)_2$  in  $\text{EC}_{0.5}:\text{PC}_{0.5}$  using (a) Ca or (b) Li RE.

of the reduction and oxidation peaks, but no such voltage hysteresis is observed (Fig. 8a). While the exact reasons for the shift are far from fully understood, processes that could contribute to it are discussed in the next section.

**Reliability of Li, Na, Mg, and Ca pseudo REs.**—REs are crucial to ensure the reliability of many electrochemical tests, but when employing non-aqueous electrolytes there is currently no consensus on appropriate REs, and hence different pseudo REs are being used, a situation which is in stark contrast to aqueous electrolytes/solutions, where numerous excellent REs exist. A good pseudo RE should present the following characteristics: non-polarizable, low impedance, reliability and reproducibility.<sup>33–35</sup> These criteria could, in principle, be met by using fast kinetics or high surface area two-phase systems.<sup>34,36</sup> While several pseudo RE candidates have been proposed over the last decade,<sup>35,37,38</sup> metallic Li remains the standard pseudo RE for Li-ion batteries and can maintain a stable potential for several days if properly cleaned.<sup>20</sup> Given the issues of Na and Ca pseudo REs in terms of potential reliability and stability, we embarked on a comparative study where the stabilities of Li, Na, Ca, and Mg metal electrodes were evaluated by assembling symmetric cells, in two-electrode configuration, and monitoring the open circuit potential (OCP) as a function of time (Fig. 9). As expected, good stability is observed for the Li cell, whereas the OCP of the Na cell fluctuates during the first 10 h and then slowly and gradually stabilizes close to 0 V. The initial fluctuations are most probably due to gas evolution during the early stages of SEI formation,<sup>23</sup> while the slow OCP stabilization can be attributed to the instability of the SEI developed on Na metal electrodes.<sup>22</sup> The

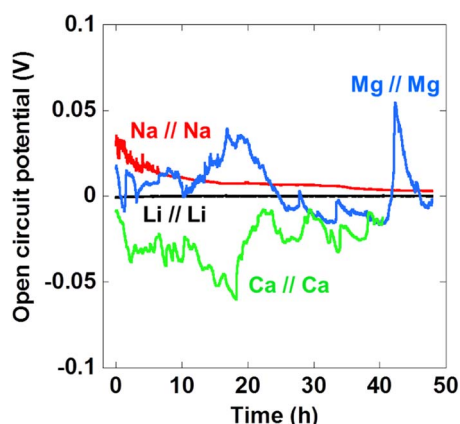


**Figure 9.** Open circuit potentials of Li, Na, Ca and Mg symmetric cells.

two divalent metal cells also displayed significant OCP oscillations, with amplitudes of ca. 40 mV, indicating that neither Ca nor Mg metal electrodes present a satisfactory stability to be used as pseudo REs.

As discussed in Reliability of Li, Na and Ca counter electrodes section, a significant potential shift was observed during Ca plating and stripping, ascribed to the Ca pseudo RE (Fig. 8). In order to better understand this phenomenon, the extent of the shift was evaluated at different temperatures: 25, 50, and 100°C, by assembling two electrode cells using Ca metal as the WE and Li metal as the CE and RE. A strong temperature dependence of the cell OCP: ca. 1.32, 1.28, and 1.04 V vs.  $\text{Li}^+/\text{Li}$  at 25, 50, and 100°C, respectively, points again at a poor potential stability (Fig. 11).

The potential shifts of the Li, Na, Mg and Ca pseudo REs were also evaluated by introducing an internal reference redox couple: ferrocenium ion/ferrocene,  $\text{Fc}^+/\text{Fc}$ , the most reliable technique for potential evaluation by CV.<sup>39</sup> The potential shifts were calculated as the difference between the observed potential of the  $\text{Fc}^+/\text{Fc}$  redox couple and its standard potential. The calculated pseudo RE potentials are reported vs. SHE for the sake of clarity (Table III). For Li and Na pseudo REs the shifts are rather small, ca. 80 and 40 mV, respectively, while for Mg and Ca they are significantly larger and strongly temperature dependent. For instance, at 25°C the calculated potential shift of the Mg and Ca pseudo REs were as large as ca. 1 and 1.4 V, respectively, corresponding to real standard potentials for Mg and Ca pseudo REs of ca.  $-1.3$  and  $-1.45$  V vs. SHE, respectively, to be compared to the expected  $-2.37$  and  $-2.87$  V vs. SHE from tabulated values.<sup>40</sup> At 100°C the shifts are smaller and the experimental standard potentials observed for Mg and Ca pseudo REs are  $-1.80$  and  $-1.81$  V vs. SHE, respectively. The calculated potential shifts from the OCPs obtained for the Ca//Li cells and from the CVs using the  $\text{Fc}^+/\text{Fc}$  internal

**Table III.** Potential shifts, determined by CV using an internal reference redox couple ( $\text{Fc}^+/\text{Fc}$ ) at 25, 50 or 100°C, for 0.1 M of  $\text{LiClO}_4$ ,  $\text{NaClO}_4$ ,  $\text{Mg}(\text{ClO}_4)_2$  and  $\text{Ca}(\text{ClO}_4)_2$  in  $\text{EC}_{0.5}:\text{PC}_{0.5}$  electrolytes.

Pseudo-RE	$E_{\text{theory}}(\text{Fc}^+/\text{Fc})$ (V)	$E_{\text{experiment}}(\text{Fc}^+/\text{Fc})$ (V)	Shift (V)	Pseudo-RE potential (V vs SHE)
$\text{Li}^+/\text{Li}$	3.44	3.36	0.08	$-2.94$
$\text{Na}^+/\text{Na}$	3.11	3.07	0.04	$-2.67$
$\text{Mg}^{2+}/\text{Mg}$	2.77	1.7 (Room T)	1.07	$-1.30$
		2.01 (50°C)	0.76	$-1.61$
		2.20 (100°C)	0.57	$-1.8$
$\text{Ca}^{2+}/\text{Ca}$	3.27	1.85 (Room T)	1.42	$-1.45$
		2.17 (50°C)	1.10	$-1.77$
		2.21 (100°C)	1.06	$-1.81$

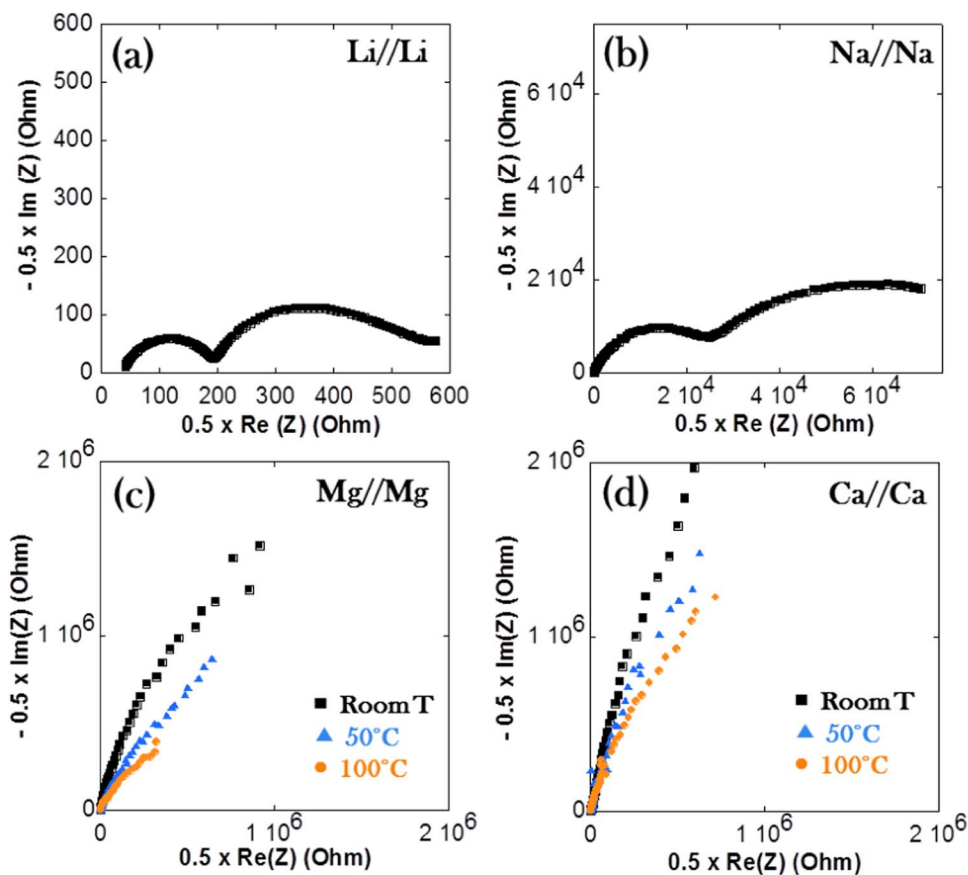


**Figure 10.** Impedance measurements (PEIS) in two-electrode configurations with 0.1 M LiTFSI, NaTFSI, Mg(TFSI)<sub>2</sub> and Ca(TFSI)<sub>2</sub> in EC<sub>0.5</sub>:PC<sub>0.5</sub> electrolytes. For the divalent cation based electrolytes a temperature study was performed at 25 (black squares), 50 (blue triangles), and 100°C (orange circles).

standard agree within 200–300 mV (Fig. 12). This remaining discrepancy is most probably associated with the potential deviation of the Fc<sup>+</sup>/Fc redox couple, depending on differences in the temperature and the solvent used.<sup>41</sup>

Although potential shifts for Ca and Mg pseudo REs have already been reported by a few groups,<sup>10,11,42</sup> with amplitudes depending on the experimental conditions, the fundamental reasons behind the phenomenon remain unclear. Here we make an attempt to evaluate four phenomena/mechanisms which possibly could contribute. First, the Nernst equation for concentrated/non-ideal electrolytes (Eq. 1) gives that an extremely low activity, and hence activity coefficient ( $\gamma_{M^{2+}}$ ), for M<sup>2+</sup> would account for strong ion-ion and ion-solvent interactions which could contribute to the potential shift.<sup>43</sup> However, even an activity coefficient as low as 10<sup>-6</sup> would result in a shift less than 200 mV and consequently cannot alone explain the shifts observed.

$$E = E^o + \frac{RT}{nF} \ln(\gamma_{M^{2+}} [M^{2+}]) \quad [1]$$

Second, the presence of another redox couple with a higher standard redox potential than the M<sup>2+</sup>/M (with M = Mg or Ca) could also influence the potential observed. However, we were unable to identify any redox couple that could display a standard potential between -2 and -1.3 V vs. SHE under our experimental conditions. The only redox couple involving Ca or Mg plausible would be M<sup>2+</sup>/M<sup>+</sup>, but this has, to the best of our knowledge, never been observed.

Third, a junction potential in the electrode vicinity, originating from poor mass transport properties of the electrolyte could lead to potential shifts. Indeed, the much higher anion transference numbers, as compared to the divalent cation, can lead to the establishment of concentration gradient during cell operation and formation of a liquid junction in the vicinity of the electrode. This phenomenon, well

known from the use of salt bridges in electrochemical cells, results in the establishment of a boundary potential difference and an electric field in the opposite direction to the migration/diffusion of the more mobile ion.<sup>44</sup> The resulting junction potential ( $E_J$ ) could be considered as an additive perturbation onto the Nernstian response ( $E_{Nernst}$ ) (Eq. 2) and cause a potential shift. In aqueous media junction potentials can extend up to a few tenths of mV, but can be expected to be larger in organic electrolytes containing divalent cation, due to the sluggish mass transport and lower cation transference number (Eq. 3).

$$E = E_{Nernst} + E_J \quad [2]$$

$$E_J = (t_+ - t_-) \frac{RT}{nF} \ln \left( \frac{a_1}{a_2} \right) \quad [3]$$

Fourth and finally, a RE with high impedance could result in a potential shift. However, in order to generate a 1 V shift for a typical input current of 50 pA at the RE, an impedance of ca. 2 × 10<sup>9</sup> Ohm would be necessary. Indeed, the Mg and Ca electrodes have very large impedances (Fig. 10), which could contribute to shifts of up to a few hundred mV, but yet they are at least one order of magnitude too small in order to alone explain the observed shifts. As a comparison, the impedance of Na metal electrodes has been reported to significantly increase upon time<sup>22</sup> and this could, at least partly, explain the continuous potential shift of the Na pseudo RE upon cycling (Fig. 6b).

Summarizing, among the four possible contributors to the potential shifts for the Ca and Mg pseudo REs, i.e. i) the activity coefficient in the Nernst equation, ii) another redox couple than M<sup>2+</sup>/M, iii) a junction potential, and iv) high electrode impedance, none can single-handedly account for the shifts observed (>500 mV). However, we

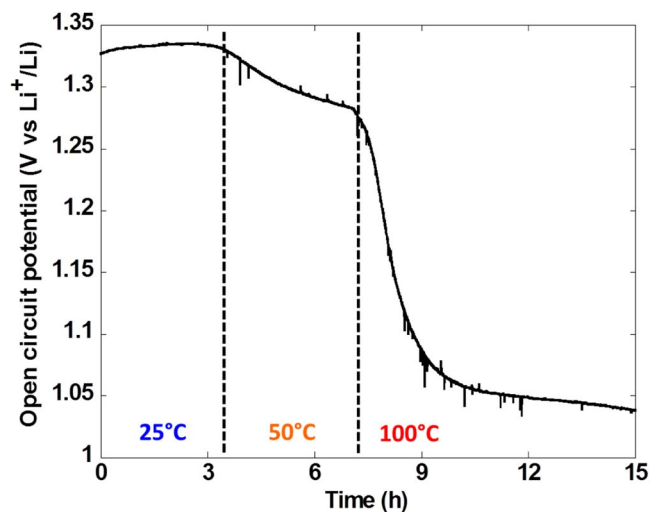


**Figure 11.** Open circuit potential of a two electrode Swagelok cell with Ca WE and Li CE and RE using 0.1 M Ca(TFSI)<sub>2</sub> in EC<sub>0.5</sub>:PC<sub>0.5</sub> electrolyte.

tentatively suggest that the experimental potential shifts are the results of a combination of these four, with the electrode impedance playing a major role.

**Monovalent vs. divalent ion transport.**—With respect to the Ca and Mg based systems this work highlights that, aside from the expected issues associated with the limited solid-state diffusion rates of divalent cations within the cathode materials,<sup>7</sup> the overall cell kinetics can also be limited by the cation transport properties within the electrolyte and also the cation desolvation at the electrolyte/electrode interface. The latter two are strongly related to the cation - anion and cation - solvent interactions, both significantly enhanced when going from monovalent to divalent cations. At a metal anode electrodeposition is commonly assumed to occur via the so-called “nucleation and growth” mechanism in a succession of steps: diffusion/migration of the complexed cation to the electrode (mass transport), adsorption with at least partial desolvation, charge transfer, surface diffusion of an adatom, and crystal growth. Each step is associated with an activation energy barrier and for Ca and Mg plating/stripping, the electrodeposition kinetics are expected to be hampered due to more energy consuming mass transport and desolvation than for monovalent cations, as outlined in recent computational studies.<sup>45–47</sup> For sake of comparison, in a Li system the desolvation was identified as the limiting step for the cation transport across the graphite anode/electrolyte interface.<sup>48</sup> From this, we foresee that the electrolyte formulation will play a major role in the development of divalent cation based batteries able to operate at low temperature and/or high power and should target the cation mobility and desolvation.

**Towards reliable electrochemical set-ups.**—In light of the findings above, reliability of electrochemical tests using Na, Ca, and Mg half-cells can only be assessed and ensured if three-electrode cell configurations are used to avoid any misleading interpretation of results. For Na cells this would also allow us to discriminate the contributions to the capacity fade of the WE and the CE, by monitoring

the potential of the latter. None of the three: Na, Ca, and Mg metal pseudo REs can be considered sufficiently reliable, and consequently there is an urgent need for development of appropriate electrochemical set-ups. Although the introduction of an internal reference redox couple (Fc<sup>+</sup>/Fc) is a most reliable technique, it cannot be performed *operando*. Other well-known pseudo REs such as Li or Ag/AgCl are possible, provided that their stability and the absence of electrolyte contamination are ensured. Indeed, a Li pseudo RE can also help in getting a rough estimate of the real potential of Ca and Mg pseudo REs under various experimental conditions. The best candidates for REs for long term cycling experiments in Na, Ca, and Mg based cells would be alloys or insertion materials presenting wide potential plateaus, two-phase systems, similar to those reported for Li cells,<sup>34,36</sup> but are not yet available at this early stage of research. Moreover, these REs should have moderate working voltages in order to avoid any passivation layer formation and hence potential instability.

## Conclusions

A comparative study on Li, Na, Ca, and Mg based electrolytes shows that results of ionic conductivity and viscosity measurements can be correlated to Raman spectra probing solvation shell and allow to assess that divalent cation (Mg or Ca) containing electrolytes suffer from significantly stronger cation-solvent and ion-ion interactions (ion pair formation) than monovalent cation, Li or Na, based electrolytes. This points at the mass transport within the electrolyte as a major issue to be carefully addressed for Ca and Mg based batteries. The electrolyte mass transport limitations and the desolvation kinetics at the electrode/electrolyte interface seem to be the two major contributors affecting the impedance of the Ca and Mg metal anodes. Possible strategies to improve cation mobility within Mg<sup>2+</sup> and Ca<sup>2+</sup> based electrolytes can include the use of anion encapsulating and cation complexing agents and careful selection of the solvent being used in order to tune the cation mobility and will be the topic of a forthcoming publication. In addition, it was demonstrated that Ca and Mg electrodes, when used as pseudo REs, are not reliable and present significant potential shifts as well as an unstable behavior, which can severely mislead the interpretation of electrochemical results. This issue appears to be mainly related to the high impedance of the electrodes and therefore experimental set-ups should be preferably based on three-electrode cell configurations. In addition to that, evaluations of the extent of the pseudo RE potential shift can and should be made using internal reference redox couple (Fc<sup>+</sup>/Fc) or other well-known pseudo REs such as Li or Ag/AgCl.

## Acknowledgments

Authors acknowledge Erlendur Jónsson for Raman activities calculations. AP has received funding from the European Research Council (ERC) under the European Union’s Horizon 2020 research and innovation programme (grant agreement No 715087). DT, MRP and AP acknowledge financial support for research on Calcium battery from Toyota Motor Europe and the Spanish Ministry of Economy and Competitiveness, through the “Severo Ochoa” Programme for Centres of Excellence in R&D (SEV- 2015-0496). DM and PJ acknowledge financial support from Honda R&D Europe for research on Magnesium battery.

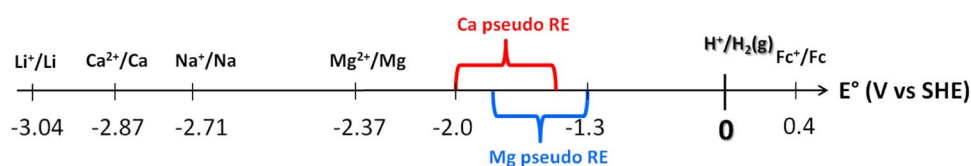


**Figure 12.** Scheme summarizing the range of potential shifts for Ca and Mg RE electrodes determined by CV using an internal reference redox couple (Fc<sup>+</sup>/Fc).

## References

1. US Geological Survey, National Minerals Information Center, Commodity Statistics and Information.
2. K. B. Hueso, M. Armand, and T. Rojo, *Energy Environ. Sci.*, **6**, 734 (2013).
3. M. D. Slater, D. Kim, E. Lee, and C. S. Johnson, *Adv. Funct. Mater.*, **23**, 947 (2013).
4. V. Palomares, M. Casas-Cabanas, E. Castillo-Martínez, M. H. Han, and T. Rojo, *Energy Environ. Sci.*, **6**, 2312 (2013).
5. N. Yabuuchi, K. Kubota, M. Dahbi, and S. Komaba, *Chem. Rev.*, **114**, 11636 (2014).
6. D. Aurbach, Z. Lu, A. Schechter, Y. Gofer, H. Gizbar, R. Turgeman, Y. Cohen, M. Moshkovich, and E. Levi, *Nature*, **407**, 724 (2000).
7. E. Levi, Y. Gofer, and D. Aurbach, *Chem. Mater.*, **22**, 860 (2010).
8. J. Muldoon, C. B. Bucur, A. G. Oliver, T. Sugimoto, M. Matsui, H. S. Kim, G. D. Allred, J. Zajicek, and Y. Kotani, *Energy Environ. Sci.*, **5**, 5941 (2012).
9. P. Canepa, G. S. Gautam, D. C. Hannah, R. Malik, M. Liu, K. G. Gallagher, K. A. Persson, and G. Ceder, *Chem. Rev.*, **117**, 4287 (2017).
10. A. Ponrouch, C. Frontera, F. Barde, and M. R. Palacín, *Nat. Mater.*, **15**, 169 (2016).
11. A. L. Lipson, B. Pan, S. H. Lapidus, C. Liao, J. Y. Vaughey, and B. J. Ingram, *Chem. Mater.*, **27**, 8442 (2015).
12. M. Cabello, F. Nacimiento, J. R. González, G. Ortiz, R. Alcántara, P. Lavela, C. Pérez-Vicente, and J. L. Tirado, *Electrochem. Commun.*, **67**, 59 (2016).
13. M. E. Arroyo-de Dompablo, C. Krich, J. Nava-Avendano, M. R. Palacín, and F. Barde, *Phys. Chem. Chem. Phys.*, **18**, 19966 (2016).
14. D. L. Proffit, T. T. Fister, S. Kim, B. Pan, C. Liao, and J. T. Vaughey, *J. Electrochem. Soc.*, **163**, A2508 (2016).
15. M. Liu, Z. Rong, R. Malik, P. Canepa, A. Jain, G. Ceder, and K. A. Persson, *Energy Environ. Sci.*, **8**, 964 (2015).
16. M. Liu, A. Jain, Z. Rong, X. Qu, P. Canepa, R. Malik, G. Ceder, and K. A. Persson, *Energy Environ. Sci.*, **9**, 3201 (2016).
17. T. Tojo, Y. Sugiura, R. Inada, and Y. Sakurai, *Electrochim. Acta*, **207**, 22 (2016).
18. M. Smeu, M. S. Hossain, Z. Wang, V. Timoshevskii, K. H. Bevan, and K. Zaghib, *J. Power Sources*, **306**, 431 (2016).
19. M. E. Arroyo-de Dompablo, C. Krich, J. Nava-Avendano, N. Biškup, M. R. Palacín, and F. Bardé, *Chem. Mater.*, **28**, 6886 (2016).
20. B. Burrows and R. Jasinski, *J. Electrochem. Soc.*, **115**, 365 (1968).
21. A. Rudola, D. Aurbach, and P. Balaya, *Electrochem. Commun.*, **46**, 56 (2014).
22. D. I. Iermakova, R. Dugas, M. R. Palacín, and A. Ponrouch, *J. Electrochem. Soc.*, **162**, A7060 (2015).
23. R. Dugas, A. Ponrouch, G. Gachot, R. David, M. R. Palacín, and J. M. Tarascon, *J. Electrochem. Soc.*, **163**, A1 (2016).
24. Z. W. Seh, J. Sun, Y. Sun, and Yi Cui, *ACS Cent. Sci.*, **1**, 449 (2015).
25. A. Ponrouch, E. Marchante, M. Courty, J. M. Tarascon, and M. R. Palacín, *Energy Environ. Sci.*, **5**, 8572 (2012).
26. M. J. Frisch, G. W. Trucks, H. B. Schlegel, G. E. Scuseria, M. A. Robb, J. R. Cheeseman, G. Scalmani, V. Barone, B. Mennucci, G. A. Petersson, H. Nakatsuji, M. Caricato, X. Li, H. P. Hratchian, A. F. Izmaylov, J. Bloino, G. Zheng, J. L. Sonnenberg, M. Hada, M. Ehara, K. Toyota, R. Fukuda, J. Hasegawa, M. Ishida, T. Nakajima, Y. Honda, O. Kitao, H. Nakai, T. Vreven, J. A. J. Montgomery, J. E. Peralta, F. Ogliaro, M. Bearpark, J. J. Heyd, E. Brothers, K. N. Kudin, V. N. Staroverov, T. Keith, R. Kobayashi, J. Normand, K. Raghavachari, A. Rendell, J. C. Burant, S. S. Iyengar, J. Tomasi, M. Cossi, N. Rega, J. M. Millam, M. Klene, J. E. Knox, J. B. Cross, V. Bakken, C. Adamo, J. Jaramillo, R. Gomperts, R. E. Stratmann, O. Yazyev, A. J. Austin, R. Cammi, C. Pomelli, J. W. Ochterski, R. L. Martin, K. Morokuma, V. G. Zakrzewski, G. A. Voth, P. Salvador, J. J. Dannenberg, S. Dapprich, A. D. Daniels, O. Farkas, J. B. Foresman, J. V. Ortiz, J. Cioslowski, and D. J. Fox, *Gaussian, Inc.* (2010), Wallingford CT.
27. M. Ender, A. Weber, and E. Ivers-Tiffée, *J. Electrochem. Soc.*, **159**, A128 (2012).
28. P. Johansson, *Phys. Chem. Chem. Phys.*, **9**, 1493 (2007).
29. J. C. Lassegues, J. Grondin, and D. Talaga, *Phys. Chem. Chem. Phys.*, **8**, 5629 (2006).
30. M. Herstedt, M. Smirnov, P. Johansson, M. Chami, J. Grondin, L. Servant, and J. C. Lassegues, *J. Raman Spectrosc.*, **36**, 762 (2005).
31. K. Xu, *Chem. Rev.*, **104**, 4303 (2004).
32. A. Benmayza, M. Ramanathan, T. S. Arthur, M. Matsui, F. Mizuno, J. Guo, P.-A. Glans, and J. Prakash, *J. Phys. Chem. C*, **117**, 26881 (2013).
33. A. Blyr, C. Sigala, G. Amatuucci, D. Guyomard, Y. Chabre, and J.-M. Tarascon, *J. Electrochem. Soc.*, **145**, 194 (1998).
34. M. Dollé, F. Orsini, A. S. Gozdz, and J.-M. Tarascon, *J. Electrochem. Soc.*, **148**, A851 (2001).
35. F. La Mantia, C. D. Wessells, H. D. Deshazer, and Yi Cui, *Electrochem. Comm.*, **31**, 141 (2013).
36. F. Mansfeld, S. Lin, Y. C. Chen, and H. Shih, *J. Electrochem. Soc.*, **135**, 906 (1988).
37. D. P. Abraham, S. D. Poppen, A. N. Jansen, J. Liu, and D. W. Dees, *Electrochim. Acta*, **49**, 4763 (2004).
38. J. L. Gómez-Cámer and P. Novák, *Electrochem. Comm.*, **34**, 208 (2013).
39. K. Izustu, in *Electrochemistry in Nonaqueous solutions*, WILEY-VCH Verlag GmbH, p. 171 (2002).
40. G. Inzelt, A. Lewenstam, and F. Scholz, in *Handbook of Reference Electrodes*, Springer Berlin Heidelberg (2013).
41. N. G. Tsierkezos, *J. Solution Chem.*, **36**, 289 (2007).
42. D. Aurbach, R. Skaletsky, and Y. Gofer, *J. Electrochem. Soc.*, **138**, 3536 (1991).
43. A. J. Bard and L. R. Faulkner, in *Electrochemical Methods: Fundamentals and Applications*, 2nd ed., JOHN WILEY & SONS, INC., p. 52, New York (2001).
44. A. J. Bard and L. R. Faulkner, in *Electrochemical Methods: Fundamentals and Applications*, 2nd ed., JOHN WILEY & SONS, INC., p. 70, New York (2001).
45. P. Canepa, G. S. Gautam, R. Malik, S. Jayaraman, Z. Rong, K. R. Zavadil, K. Persson, and G. Ceder, *Chem. Mater.*, **27**, 3317 (2015).
46. M. Okoshi, Y. Yamada, A. Yamada, and H. J. Nakai, *J. Electrochem. Soc.*, **160**, A2160 (2013).
47. M. Okoshi, Y. Yamada, S. Komaba, A. Yamada, and H. Nakai, *J. Electrochem. Soc.*, **164**, A54 (2017).
48. K. Xu, A. von Cresce, and U. Lee, *Langmuir*, **26**, 11538 (2010).